Evaluation of *in vitro* and *in vivo* biocompatibility of iron produced by powder metallurgy

Thaís Casagrande Paim[a,1], Diego Pacheco Wermuth[b,1], Isadora Bertaco[a], Carla Zanatelli[a], Liliana Ivet Sous Naasani[a], Mônica Slaviero[c], David Driemeier[c], Lirio Schaeffer[b,2], Márcia Rosângela Wink[a,*,2]

[a] *Laboratório de Biologia Celular, Departamento de Ciências Básicas da Saúde, Universidade Federal de Ciências da Saúde de Porto Alegre (UFCSPA), Rua Sarmento Leite 245, 90050-170 Porto Alegre, RS, Brazil*
[b] *Laboratório de Transformação Mecânica, Universidade Federal do Rio Grande do Sul (UFRGS), Av. Bento Gonçalves 9500, 91501-970 Porto Alegre, RS, Brazil*
[c] *Setor de Patologia Veterinária, Faculdade de Veterinária (FAVET), Universidade Federal do Rio Grande do Sul, Av. Bento Gonçalves 9090, 91540-000 Porto Alegre, RS, Brazil*

A B S T R A C T

Biodegradable metallic materials (BMMs) are expected to corrode gradually in vivo after providing the structural support to the tissue during its regeneration and healing processes. These characteristics make them promising candidates for use in stents. These endoprostheses are produced from metal alloys by casting and thermomechanical treatment. Since porous alloys and metals have less corrosion resistance than dense ones, the use of powder metallurgy becomes an option to produce them. Among the metals, iron has been proposed as a material in the manufacturing of stents because of its mechanical properties. However, even then it is unclear what toxicity threshold is safe to the body. Thus, the objective of this research was to verify the biocompatibility of sintered 99.95% and 99.5% pure iron by powder metallurgy in vitro with Adipose-derived mesenchymal stromal cells (ADSCs) and in vivo with a Wistar rat model. Herein, characterizations of iron powder samples produced by the powder metallurgy and the process parameters as compression pressure, atmosphere, sintering time and temperature were determined to evaluate the potential of production of biodegradable implants. The samples obtained from pure iron were submitted to tests of green and sintered density, porosity, microhardness, hardness and metallography. The biocompatibility study was performed by indirect and direct cell culture with iron. The effects of corrosion products of iron on morphology, viability, and proliferation of ADSCs were evaluated in vitro. Hemolysis assay was performed to verify the hemocompatibility of the samples. In vivo biocompatibility was evaluated after pure iron discs were implanted subcutaneously into the dorsal area of Wistar rats that were followed up to 6 months. The results presented in this paper validated the potential to produce biodegradable medical implants by powder metallurgy. Both iron samples were hemocompatible and biocompatible in vitro and in vivo, although the 99.95% iron had better performance in vitro than 99.5%.

1. Introduction

Biodegradable metallic materials (BMMs) are expected to corrode gradually *in vivo* after providing the structural support to the tissue during its regeneration and healing processes. The major components of BMMs should be essential metallic elements that can be metabolized by the organism with appropriate degradation rates to avoid overload. Magnesium-based BMMs and Iron-Based BMMs are the most commonly proposed metals to be used in cardiovascular or orthopedic implants [1,2].

In cardiovascular applications, BMMs are promising candidates for use in stents, whose main function is to keep the lumen open after the angioplasty procedure [3,4]. The ideal biodegradable cardiovascular stent must be biocompatible, prompt to disappear without developing an inflammatory response and it should have mechanical properties providing the required support to the vessel during the necessary period. The degradation must begin at a very slow rate to keep the mechanical integrity of the stent until the arterial vessel remodeling, which is expected to conclude in a period of 6–12 months [5–7].

Most of the cardiovascular stents including BMMs are produced from metallic ingots fabricated using both casting and thermo-mechanical treatment. Recently, the use of new processes in the fabrication of biodegradable metallic stents, such as powder metallurgy, has been investigated. Because porous alloys and metals normally have less corrosion resistance than fully dense alloys, the use of powder metallurgy became a promising option in the conception of biodegradable stents [3,8].

The conventional process of powder metallurgy consists of metal

forming metallic powders, alloy powders and non-metallic materials or ceramic powders in reliable parts, within a tool of the desired shape by applying pressure. The parts made by powder metallurgy have a certain porosity, which can be controlled by factors such as compaction pressure, sintering temperature and time, size and shape of the powder particles [4]. The resulting porosity provides greater degradability that can reduce the absorption time of the implant in the organism because of its larger surface area [9]. In addition, this process allows a controlled porosity. This feature would facilitate the adherence of drugs that can be useful to produce drug-eluting stents [10].

Among the BMMs, iron has been proposed as an adequate material in the manufacturing of stents because its mechanical properties are closer to stainless steel 316L (SS316L) than the Mg alloys are. This provides higher confidence for stent application, which requires high strength and ductility [11]. Besides, iron has other benefits for clinical applications: it is essential to human life, possesses low toxicity and the transport mechanisms for clearance of its degradation products are relatively understood. However, its excess can be deleterious [12]. An iron overload may be caused by a continuous load of iron that exceeds 1–2 mg/day. It happens due to the lack of active excretion pathways for iron in the human body, which may lead to organ failures [12]. Henceforth, the level of degradation of an intravascular device composed of this element must be well-known.

It has been discussed that the level of impurities occurring in each production step needs to be determined. However, it is still unclear what level of impurity concentration is considered tolerable, and thus may be left in the material to maintain the device properties. Therefore, in the present study, we produced sintered iron samples with 99.95 and 99.5% of purity by powder metallurgy (99.95 and 99.5% iron) and evaluated *in vitro* and *in vivo* biocompatibility of the biomaterial for future applications in biomedical devices.

2. Materials and methods

2.1. Iron powder samples

The iron powders used in this study have a purity of 99.95% (Lyuelong superfine metal Co., China) and 99.5% (TCK, Yeoui-aero, Korea).

The chemical analysis with the maximum percentages of the elements to guarantee the purity of the powders was provided by the suppliers. Table 1 shows the limits of the elements contained in the powders used in this research.

Scanning Electron Microscope (SEM) was employed to assess the morphology of the iron powders and the granulometry test was performed to determine the particle size distribution.

2.2. Iron samples with 99.95 and 99.5% of purity obtained by powder metallurgy

The samples were compacted by a cylindrical die of tempered steel AISI D6 in manual hydraulic press with a maximum capacity of 30 tons. The compacted samples for *in vitro* experiments measured approximately 13.0 mm in diameter (Ø) and 11.0 mm in height (h) and the samples used for *in vivo* implantation measured approximately 6.5 mm in diameter (Ø) and 2.0 mm in height (h). In this study, the compaction pressure used was 600 MPa.

To calculate the density of the compacted samples, the masses were

weighed on an analytical balance and the diameters and heights were measured using a micrometer. The sintering was performed in an electric tube furnace silicon carbide resistor, with electronic control, precision $\pm$ 1 °C at the working temperature and atmosphere of Argon. The sintering cycle used was 1150 °C for 60 min and the cooling was carried out in the oven. The density of the sintered samples was measured in the same way as the compacted samples.

Mechanical properties analyses of the sintered pure iron samples were performed. The microhardness and hardness were measured using Vickers and Brinell tests, respectively. The Vickers hardness of the sintered pure iron samples was determined by durometer Insize ISH-TDV 1000 with load of 0.5 kgf (4.9 N), according to ASTM E384 [13]. The Brinell hardness was determined by hardness tester MRS Fortel with 2.5 mm diameter indenter and a load of 62.5 kgf (612.92 N), according to ASTM E10 [14]. The sintered metallography was performed according to standard preparation and polishing. The samples were abraded with sandpaper aluminum oxide 100, 200, 400, 600, 800, 1000 and 1200 "mesh" being polished with diamond paste 1 μm and observed by an optical microscope [15].

The ImageJ software was used to improve the quality of the images and evaluate the porosity and the grain size, after the etching by 2% Nital reagent, according to ASTM E 562-02 standard [16].

2.3. Adipose-Derived Stem Cells: Isolation and characterization

Adipose-Derived Stem Cells were extracted from the abdominal adipose tissue of a healthy adult donor undergoing tumescent liposuction. The experimental protocol was approved by the Research Ethics Committee of Santa Casa de Misericórdia of Porto Alegre (ISCMPA) and Research Ethics Committee of the Federal University of Health Sciences of Porto Alegre (UFCSPA) (approval no. 3029.141 and 3.734.612, respectively). The written informed consent was obtained from donors according to the Declaration of Helsinki. The isolation and culture of ADSCs were performed as previously described by our group [17,18].

Briefly, the tissue was washed with phosphate-buffered saline (PBS) and its extracellular matrix was digested with type I collagenase solution (250 U/mg, 1 mg/mL) at 37 °C for 30 min with periodic shaking. The enzymatic action was neutralized with the addition of Dulbecco's modified Eagle's Medium standard (DMEM)- low glucose (Sigma-Aldrich, St. Louis, USA), supplemented with 10% FBS (Fetal Bovine Serum). Cells were centrifuged at 1200 rpm for 10 min and the supernatant was discarded. Subsequently, they were resuspended in erythrocyte lysis buffer (150 mM NH_4Cl, 10 mM $NaHCO_3$ and 1 mM EDTA) with simultaneous mechanical shaking and incubated for 15 min at room temperature.

The solution was centrifuged at 1200 rpm for 10 min, a procedure that separates the adipocytes present in the supernatant of the vascular stroma cell fraction (SVF), which consists of a heterogeneous population of cells, including circulating blood cells, fibroblasts, pericytes, endothelial cells, and it is also rich in MSCs. Cells present in the pellet were cultured with the standard medium supplemented with 10% FBS, 100 U L^{-1} penicillin and 100 mg/L streptomycin. It was kept in an aseptic and humidified environment at 37 $\pm$ 0.1 °C and 5% CO_2 and routinely passaged at preconfluency using 0.25% trypsin and 0.01% EDTA. For the experiments, cell cultures were used in passages from 4 to 10 [17].

These cells were tested to verify their capabilities to differentiate into adipogenic, chondrogenic and osteogenic cells. The adipogenic and osteogenic differentiation were induced according to Beckenkamp et al., 2018 [19]. Briefly, adipogenesis induction medium (AIM) contained DMEM with high glucose, 10% FBS, 1 μM dexamethasone, 10 μg/L insulin, 200 μm indomethacin, osteogenic induction medium (OIM) contained DMEM with high glucose, 10% FBS, 0.1 uM dexamethasone, 10 mM β-glycerol phosphate, and 200 μM ascorbic acid and StemPro® Chondrogenesis Differentiation Kit (Gibco®; Invitrogen, Grand Island, NY) were used in the experiment. The differentiated cells

Table 1
Maximum percentage of elemental impurities.

Fe %	C %	H %	N %	S %	O %
≥99.95	≤0.02	–	–	≤0.01	≤0.02
≥99.5	≤0.15	≤0.1	≤0.01	≤0.19	≤0.05

were observed by Oil Red O, Alcian blue and Alizarin Red Staining.

Cells were characterized by immunophenotyping on the FACSCalibur flow cytometer (BD Bioscience, USA) using a cytometric buffer, containing the monoclonal antibodies PE-anti CD14, FITC- anti CD34, PE- anti CD45, FITC- anti CD44, PE- anti CD105 (Invitrogen™, Waltham, MA, USA), PE- anti CD90 (Biolegend), and CD73 proteins (BD Pharmingen™). MSCs derived from adipose tissue express the typical markers of mesenchymal cells, such as CD44, CD73, CD90 and CD105, and poorly express markers of hematopoietic and endothelial lineages: CD14, CD34 and CD45 [20]. At least 10,000 events were collected using a FACSCalibur flow cytometer equipped with a 488-nm argon laser, BD CellQuest software (Becton-Dickinson, San Diego) and they were analyzed using FlowJo Software.

2.4. Indirect contact tests

2.4.1. Iron extract

Sintered pure iron samples were autoclaved and incubated for 24 h and 48 h in the culture medium, in a humidified atmosphere with 37 ± 0.1 °C and 5% CO_2. The surface area/extraction medium ratio was 1.25 cm^2/mL, in accordance with the EN ISO 10993-12. At the end, the 24 h and 48 h iron extract were collected, sterilized in 0.22 μm membranes and used to treat cells for 24 h and 48 h, respectively [21].

2.4.2. Indirect cytotoxicity testing (MTT assay)

The effects of corrosion products of Fe ion concentration on ADSCs cells were determined by MTT assay (3-(4,5-dimethylthiazol-2-yl)-2,5-diphenyltetrazolium bromide). This method was used to measure the viability of cells with iron extract. Cells were seeded in a 96-well plate at a ratio of 3.0×10^3 cells per well and incubated at 37 ± 0.1 °C and 5% CO_2. After one day, the medium was removed, and the cells were treated with supernatants containing Fe ions. For this assay, 100% extract was diluted with DMEM 10% FBS to 10%, and 1%. ADSCs with standard media were used as a negative control. After that, the medium was aspirated and replaced with a fresh standard medium containing MTT (5 mg/mL) for 3 h at 37 °C. After incubation, the supernatant was carefully aspirated from each well, followed by solubilization with dimethyl sulfoxide (DMSO). The absorbance of the specimens was measured with a multi-detection microplate reader SpectraMax M2 (Molecular Devices Corporation, USA) at 560 nm and the cell viability index was calculated from the ratio of the optical density of the extracts to the optical density of control.

2.4.3. Sulforhodamine B

The sulforhodamine B (SRB) assay is used to investigate cell proliferation, based on the measurement of cellular protein content [22,23]. The methods of seeding and treatment were identical to the MTT assay. ADSCs with standard media were used as a negative control.

After incubation, cells were fixed by protein precipitation with 50% trichloroacetic acid at 4 °C for 45 min. After washing with water, the cells were stained for 25 min with 0.4% SRB dissolved in 1% acetic acid and subsequently washed with 1% acetic acid to remove unbound dye. The plate was air-dried and bound protein stain was solubilized with 10 mM Tris base [tris(hydroxymethyl)aminomethane]. The optical density was read at 530 nm.

2.4.4. DAPI and Phalloidin stain

To verify nuclear and actin cytoskeletal morphology of cultured cells with 100% iron extract, they were stained with 4′,6-diamidino-2-phenylindole (DAPI) (Molecular Probes) and Alexa 488 phalloidin (Sigma). For this purpose, the ADSCs were seeded in 12-well plates with a culture medium ratio of 2×10^4 cells per well and treated with the iron extracts. ADSCs seeded on the cell culture plate with standard media were used as a negative control. After 24 h and 48 h, the treatment was removed and the cells were washed with PBS $1 \times$. Then, they

were fixed with 4% paraformaldehyde for 30 min, permeabilized with Triton X-100 (0.1%) for 20 min and labeled with phalloidin (for filamentous actin) and DAPI (for nuclear DNA) during 40 min. After staining, the cells were visualized in the Olympus BX50 Fluorescence microscope coupled to a Motican 2500 camera (Olympus, Hamburg, Germany).

2.5. Direct culture on sintered iron samples

ADSCs were seeded on sintered iron samples at a ratio of 3×10^4 cells per disc and incubated at 37 ± 0.1 °C and 5% CO_2 for 24 h. After, cells were stained with DAPI and phalloidin as previously described.

2.6. Hemolysis assay

The hemolysis assay was performed to evaluate the hemocompatibility of the iron samples (99.95 and 99.5%). It was carried out according to Mota Ferreira et al. 2016, with some modifications [24].

The blood was obtained from healthy human volunteers, upon approval by the Research Ethics Committee of UFCSPA (approval no. 3.594.874). Blood samples were centrifuged and 1 mL of erythrocytes was diluted 10 times with $1 \times$ PBS. The iron samples were covered with 10 mL blood solution. For negative control, blood was incubated with $1 \times$ PBS and for positive control with distilled water. Iron, positive and negative control samples were incubated for 30 min, 1, 2 and 3 h at 37 °C and blood supernatants were centrifuged at 1200 rpm for 5 min. The reaction product was analyzed by measuring absorbance at 540 nm and the hemolysis percentage was calculated using the following equation [25]:

$$\text{Hemolysis}(\%) = \frac{\text{OD (sample)} - \text{OD (negative control)}}{\text{OD (positive control)} - \text{OD (negative control)}} \times 100\%$$

where, O.D.(sample), O.D.(negative control) and O.D.(positive control) are the optical densities of the test sample, the negative control and the positive control, respectively. All data were calculated based on the average of four or more replicates.

2.7. In vivo biocompatibility of iron

2.7.1. Murine subcutaneous implantation preclinical model

For the *in vivo* analysis of biocompatibility, pure iron discs were implanted subcutaneously into the dorsal area of *Wistar* rats. All experimental procedures were approved by UFCSPA Animal Ethics committee (approval no. 613/19). For this study 52 female rats Wistar with $\pm$ 8 weeks and an average body weight of 209 g were randomly allocated to three groups for the 1 week, 3 and 6 months time points investigated. Each group was randomly divided into three other groups, according to treatment. The animals were anesthetized *via* intraperitoneal (IP) injection with an association of 90 mg/kg ketamine and 10 mg/kg xylazine. Two groups received a subcutaneous implant of either pure iron discs (99.95 or 99.5% iron). The Sham group (control) received the same surgical procedure, but not implantation of discs. After the implantation of the discs, analgesic relief was provided for two days (12/12 h) by subcutaneous administration of Tramadol Hydrochloride.

The rats were monitored daily during the first two weeks for surgical wound appearance and general well-being. An evaluation of body weight gain was performed monthly. After 1 week, 3 and 6 months, the rats were euthanized by cardiac exsanguination, blood was collected for hematological and serum analysis, followed by implant and tissue harvest.

2.7.2. Blood and serum analysis

The whole blood was collected in the EDTA tube for red blood cell (RBC), white blood cell (WBC) counts and for determining hemoglobin

(HGB) levels. The hematologic analyses of non-coagulated blood samples were performed in BC-5380 auto hematology analyzer (Mindray, Shenzhen, China). Serum from separation tube was used to assess the levels of aspartate aminotransferase (AST), Alkaline phosphatase (ALP), Alanine transaminase (ALT), ferritin and iron (Bioclin® Kits, Brazil). The analyses were performed in the BS-120 chemistry analyzer (Mindray, Shenzhen, China).

2.7.3. Histological analysis

The implants with surrounding tissue were recovered, carefully separated from the tissue, dried, ultrasonicated for 20 min immersed in alcohol, cleaned, air-dried, and the final mass was measured to determine the change in mass. The tissue around the implant location and organs (liver, heart, lungs, spleen and kidney) were fixed in 10% neutral buffered formalin for histological assessment. They were trimmed, included in paraffin, sectioned (4 um per section) and deparaffinized on microscopy slides. Finally, tissue samples were stained with hematoxylin and eosin (H&E), and analyzed by a veterinary pathologist to identify inflammatory infiltration, fibrosis and necrosis.

2.8. Statistical analysis

Statistical analysis was conducted with GraphPad Prism biostatistics software (GraphPad Inc., California, USA). Differences between groups were analyzed using two-way ANOVA. $p < 0.05$ was accepted as a statistically significant difference between means. Error bars within figures represent standard errors.

3. Results and discussion

In this study, 99.95% and 99.5% iron samples were produced by powder metallurgy. The physical and mechanical characteristics were analyzed by green density, sintered density, porosity, microhardness (HV), hardness (HB) and metallography. The biocompatibility of these samples was tested *in vitro* using primary mesenchymal stromal cells from adipose tissue and *in vivo* using an animal model.

3.1. Physical and mechanical properties

The SEM micrographs analysis of the iron powder with a purity of 99.95% and 99.5% shows the metal morphology at $10000\times$ magnification (Fig. 1). It can be observed that the iron powder samples have a nearly-spherical shape with a homogeneous distribution of particle sizes. The powder samples have this morphology due to its production process by atomization. In addition, the surface of 99.95% iron powder

is smooth (Fig. 1A) and the 99.5% iron powder has protrusions (Fig. 1B). Both purities of iron powders have a diameter ranging between 1 and 5 μm.

Considering that the size of particles is crucial to the manufacturing of sintered components [26], the granulometry test of iron powders was performed (Fig. 2). The average particle size found is 5.75 μm and 7.47 μm, for 99.95% and 99.5% iron, respectively. The results of Fig. 2 are summarized in Table 2.

The green density of the iron compacted samples with 99.95% of purity showed an average green density of 6.6 g/cm^3 and variation between 6.5 and 6.7 g/cm^3. The compacted samples with 99.5% of purity showed an average green density of 5.65 g/cm^3 and variation between 5.5 and 5.7 g/cm^3. As it can be seen, there is a difference between the green densities of the samples because the 99.95% iron powder has greater compressibility than 99.5%. This is probably due to the protuberances found in 99.5% iron particles, shown in Fig. 1B.

The densities of both purities of iron were similar after sintering. The average density of 99.95% and 99.5% sintered pure iron samples reached 6.5 g/cm^3 $\pm$ 0.2 (6.5 to 6.7 g/cm^3 for 99.95% and 6.3 to 6.5 g/cm^3 for 99.5%) in the pressure of 600 MPa, a satisfactory result for the material.

The sintered samples were further evaluated by metallography. The Fig. 3 shows 99.95% and 99.5% iron samples, before (Fig. 3A and C) and after (Fig. 3B and D) etching by Nital 2%. The 99.95% iron (Fig. 3A) showed small pores measuring between 1.1 and 7.9 μm, and larger pores between 13.7 and 30.7 μm (average size 2.3 μm); while 99.5% iron (Fig. 3C) showed small pores measuring between 1.1 and 8.8 μm, and larger pores between 17.6 and 31.1 μm (average size 2.9 μm). Considering the pores average size measured in both samples, they can be considered as small pores.

The iron sintered samples have a porosity whose characteristic is directly related to the density. However, both samples showed a similar density, with an average of 17.41%, lesser than the theoretical density. The variation of density to 99.95% and 99.5% sintered pure iron samples was 0.4 g/cm^3 (6.5 to 6.7 g/cm^3 for 99.95% and 6.3 to 6.5 g/cm^3 for 99.5%).

The analysis of grain sizes showed that both samples presented several grain sizes. The average grain size measured in the 99.95% iron samples was 19.94 μm $\pm$ 13.06 (Fig. 3B). The 99.5% iron samples had an average grain size of 34.45 μm $\pm$ 15.08 (Fig. 3D). These grain sizes and variations have adequate mechanical properties for medical applications [27].

As mechanical tests, we have chosen to perform the Vickers microhardness (HV) and Brinell hardness (HB) tests. The microhardness measured of 99.95% and 99.5% iron samples were 185.8 HV $\pm$ 17.9
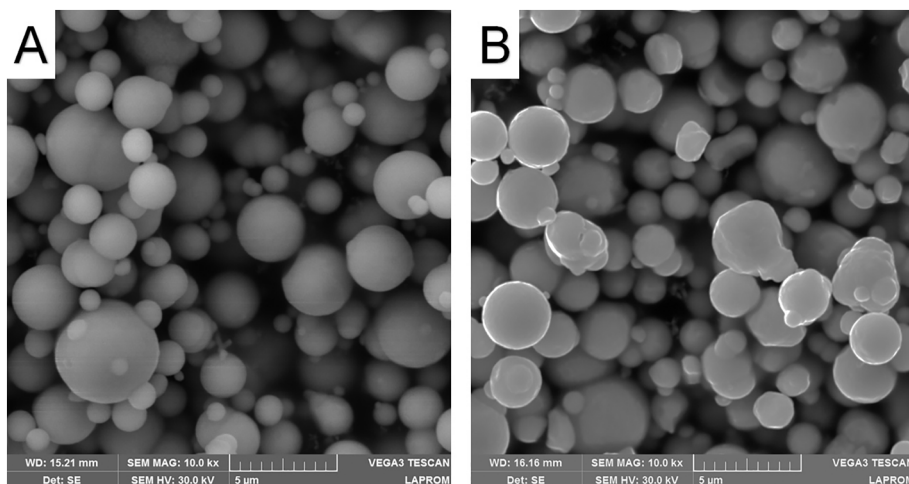

Fig. 1. SEM micrographs of the iron powder morphology with a purity of 99.95% (A) and 99.5% (B).
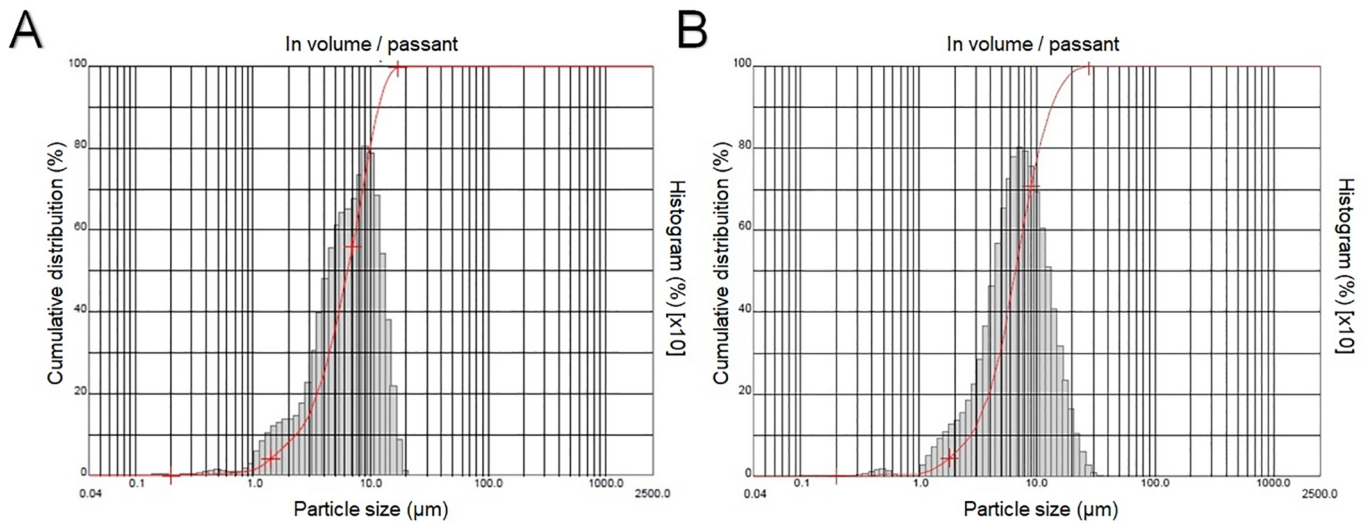
Fig. 2. Particle size distribution of 99.95% (A) and 99.5% (B) iron powder.

Table 2
Particle size analysis of 99.95% and 99.5% iron powders.

	99.95% Iron	99.5% Iron
D90	< 11.69 μm	< 13.36 μm
D50	< 6.33 μm	< 6.61 μm
D10	< 2.3 μm	< 2.70 μm
Average particle size	5.75 μm	7.47 μm

(1822 MPa) and 180.2 HV ± 12.7 (1767 MPa), respectively. These values were close to 317 L stainless steel, 198.7 HV ± 9.9 (1949 MPa), which is considered the golden standard to the manufacture of permanent stents [28]. The Brinell hardness test showed homogeneity in measured values, 99.95% iron samples had 64.4 HB ± 0.6 and 99.5% iron samples had 62.1 HB ± 1.7. These results are equivalent to those found in biomedical magnesium alloys applied *in vivo* stent studies with rabbit models [29]. In conclusion, the 99.95% iron samples have greater hardness and microhardness than 99.5% iron samples, which can be due to the pores and grains of the smaller microstructure.

3.2. Isolation and characterization of ADSCs

MSCs isolated from human adipose tissue showed a typical fusiform morphology, adherence to plastic, capacity to self-renew and
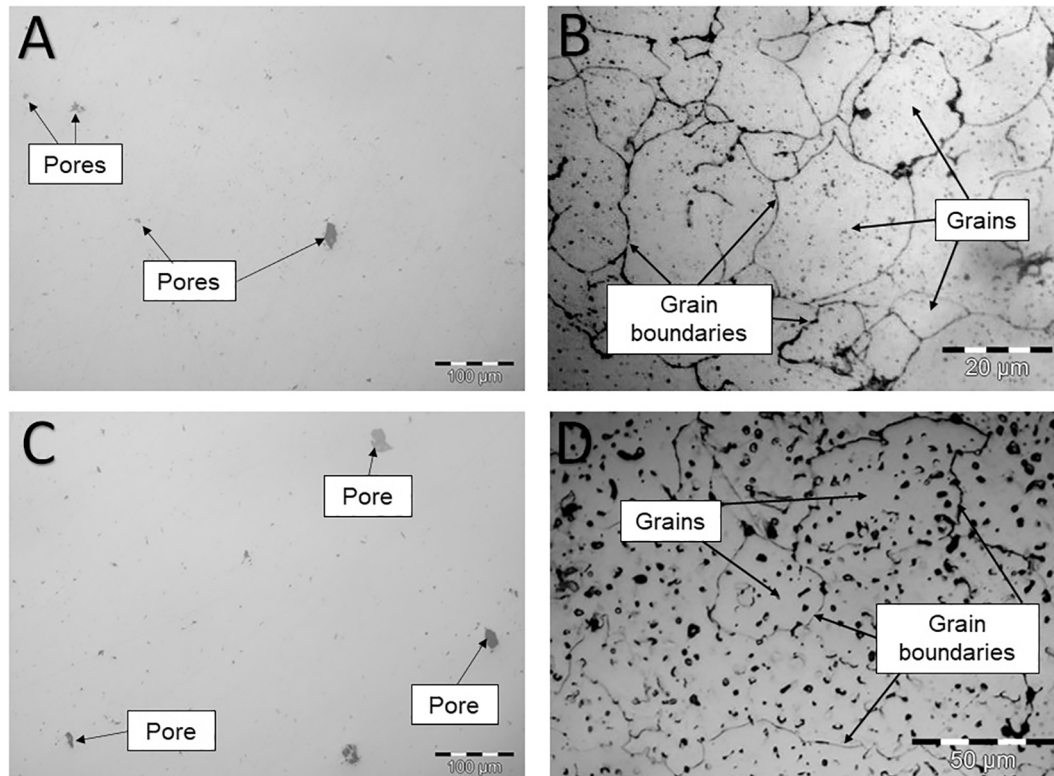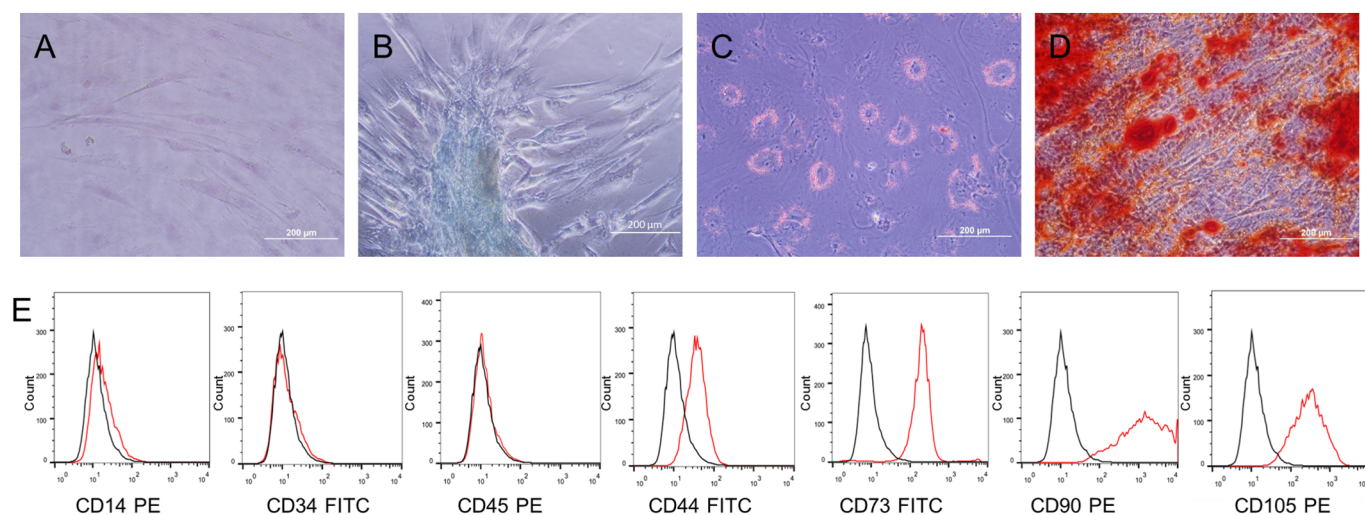

Fig. 3. Metallography of 99.95% sintered iron without etching, 200× magnification (A) and after etching of Nital 2%, 1000× magnification (B); 99.5% sintered iron without etching, 200× magnification (C) and after etching of Nital 2%, 500× magnification (D).

Fig. 4. Characterization of Adipose Derived Stem Cells (ADSCs). (A) Non differentiated control cells. (B–D) Cells show potential for differentiation towards chondrogenic (Alcian Blue), adipogenic (Oil Red O staining) and osteogenic (Alizarin Red) lineages. (E) Flow cytometry of ADSCs shows that cells were negative for CD14, CD34 and CD45 and positive for CD44, CD73, CD90 and CD105. Optical microscopy, 200× magnification.
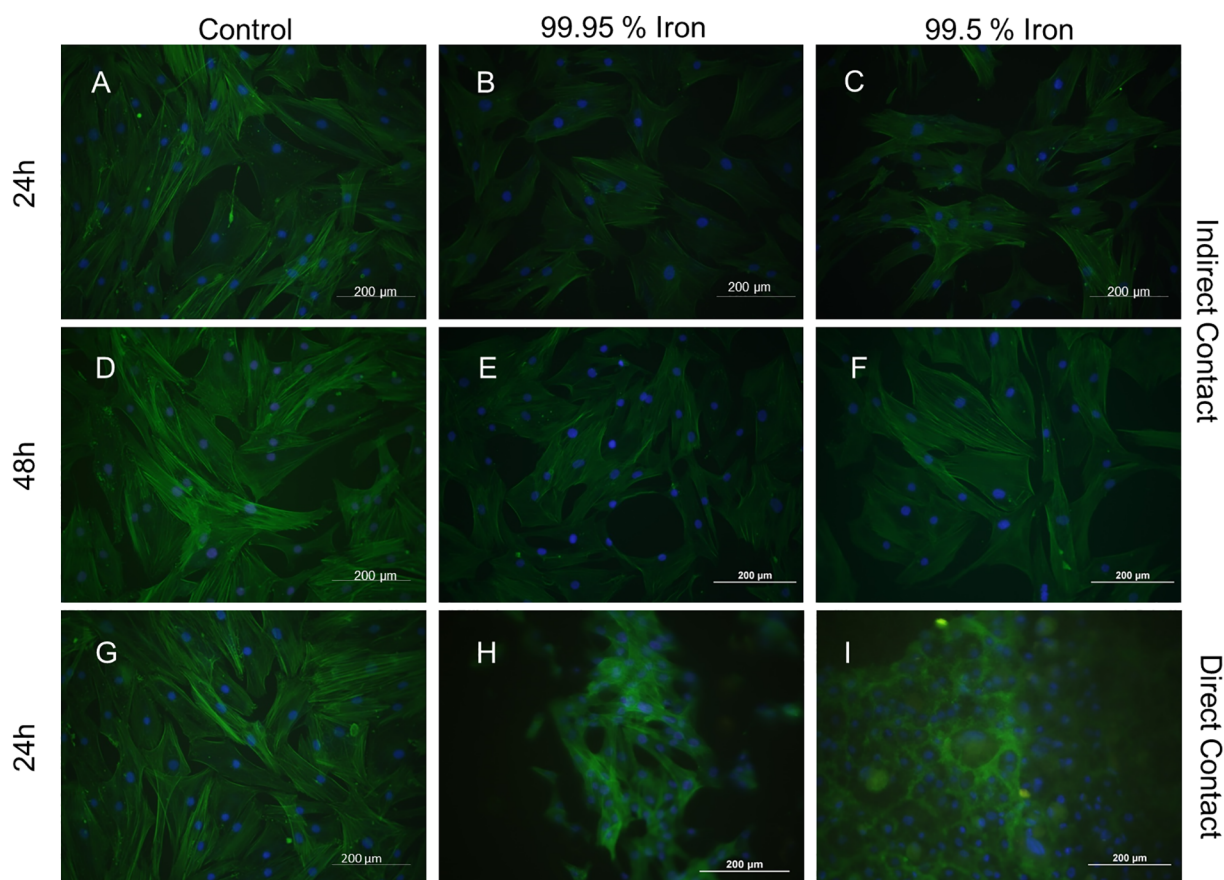
Fig. 5. Micrographs show the F-actin cytoskeleton (green) and nuclei (blue) of the ADSCs treated with 99.95 and 99.5% iron extract of 24 and 48 h for, respectively, the same time (B, C, E, F) and negative control (A, D, G). Fluorescence microscopy, 200× magnification.

differentiate *in vitro*. The immunophenotyping results by flow cytometry indicated that cells were positive for the mesenchymal stem cell markers CD44, CD73, CD90 and CD105 but negative for the hematopoietic cell markers CD14, CD34 and CD45. They were also able to differentiate in three cellular lineages: chondrogenic, adipogenic and osteogenic when stimulated with differentiation medium. The intracellular lipid vacuoles in adipocytes were identified with Oil Red O solution, the biosynthesis of proteoglycans by chondrocytes with alcian

blue and the calcium-rich mineralized matrix in osteocytes with alizarin red S staining. These characteristics confirm that the cultured cells are phenotypically mesenchymal as well as functionally multipotent (Fig. 4) [30].

3.3. In vitro biocompatibility

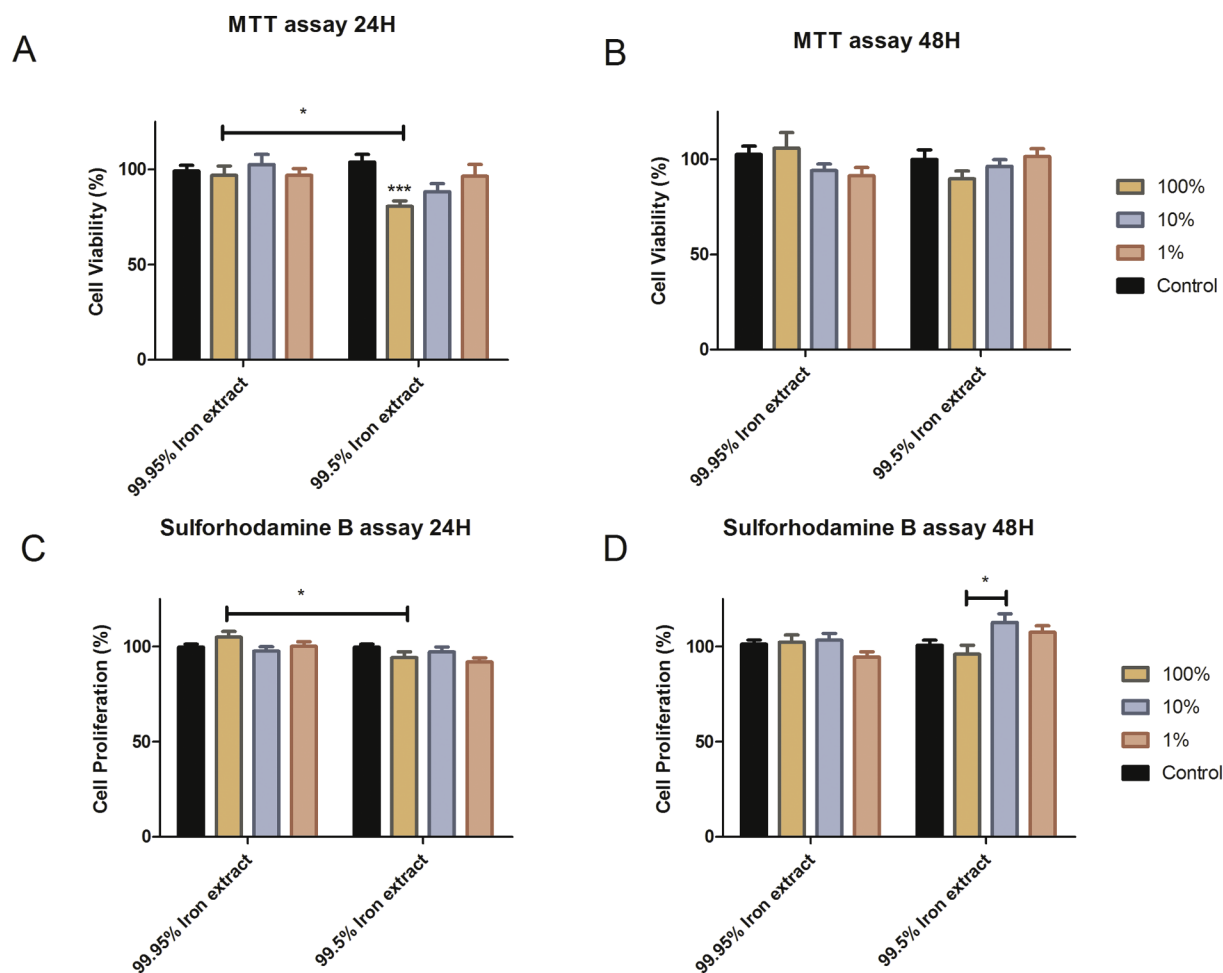*In vitro* cytocompatibility was assessed on the 99.95 and 99.5%

Fig. 6. Graph representing the cell viability (A–B) and proliferation (C–D) after culture with 99.95 and 99.5% iron extracts for 24 h and 48 h. N = 3 *represents p < 0.05.
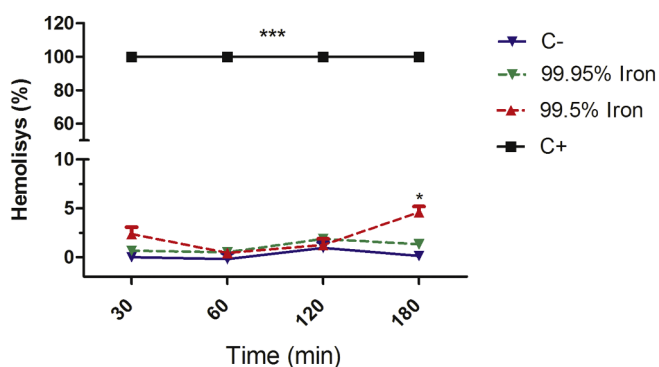

Fig. 7. Hemolysis percentages of 99.5 and 99.95% iron samples after 30, 60, 120 and 180 min. Water was used as positive control and $1\times$ PBS as negative control. N = 3. *represents p < 0.05.

sintered iron samples by (1) analyzing the cytomorphology with DAPI-Phalloidin stain after growing cells using the iron extracts or by directly plating them on the iron discs (Fig. 5); and by (2) exposing ADSCs to media containing degradation products of the materials and analyzing cell viability and proliferation, using the colorimetric MTT assay and Sulforhodamine B, respectively (Fig. 6).

Cells cultured with 99.95% and 99.5% iron extracts showed adherence to plastic and the typical fusiform morphology of the ADSCs. They also maintained the integrity of the actin cytoskeleton and nuclei as observed by fluorescence microscopy (Fig. 5A–F). Regarding the cells

that were directly plated on the surfaces of iron discs, they were able to adhere and grow. The morphology of ADSCs plated on 99.95% iron disc did not change, in contrast to cells cultured on 99.5% iron that suffered alteration in the fibroblastic morphology due to the disorganization of their actin filaments (Fig. 5G–I).

In addition, the MTT assay results exhibited good cytocompatibility with 100%, 10% and 1% iron extracts in 24 h and 48 h, as shown in Fig. 6A–B. ADSCs presented similar viability when they were compared to the negative control, although the cells cultured with 100% extract of 99.95% iron were statistically more viable than those cells treated with 99.5% after 24 h. SRB assay showed that cells did not lose their proliferation potential after 24 h and 48 h of incubation with iron extracts. Interestingly, when cells were treated for 24 h with 100% extract of 99.95% iron, they were more proliferative than with 99.5% (p < 0.05) (Fig. 6C–D).

According to ISO 10993-5 if viability is reduced by > 30%, the biomaterial has a cytotoxic potential. Based on this recommendation, both iron extracts caused no cytotoxic effect on ADSCs in our analysis. In accordance, degradation products of iron with different levels of purity and its alloys *i.e.*, iron-oxides, hydroxides, carbonates, and phosphates, have also been reported to be non-toxic and cytocompatible to fibroblast [6,31] endothelial [32,33], smooth muscle [33,34] and mesenchymal [31] cells [35,36].

3.4. Hemocompatibility in vitro

The hemolysis assay was applied for evaluating the hemocompatibility of iron samples. The ASTM F756-08 materials can be classified
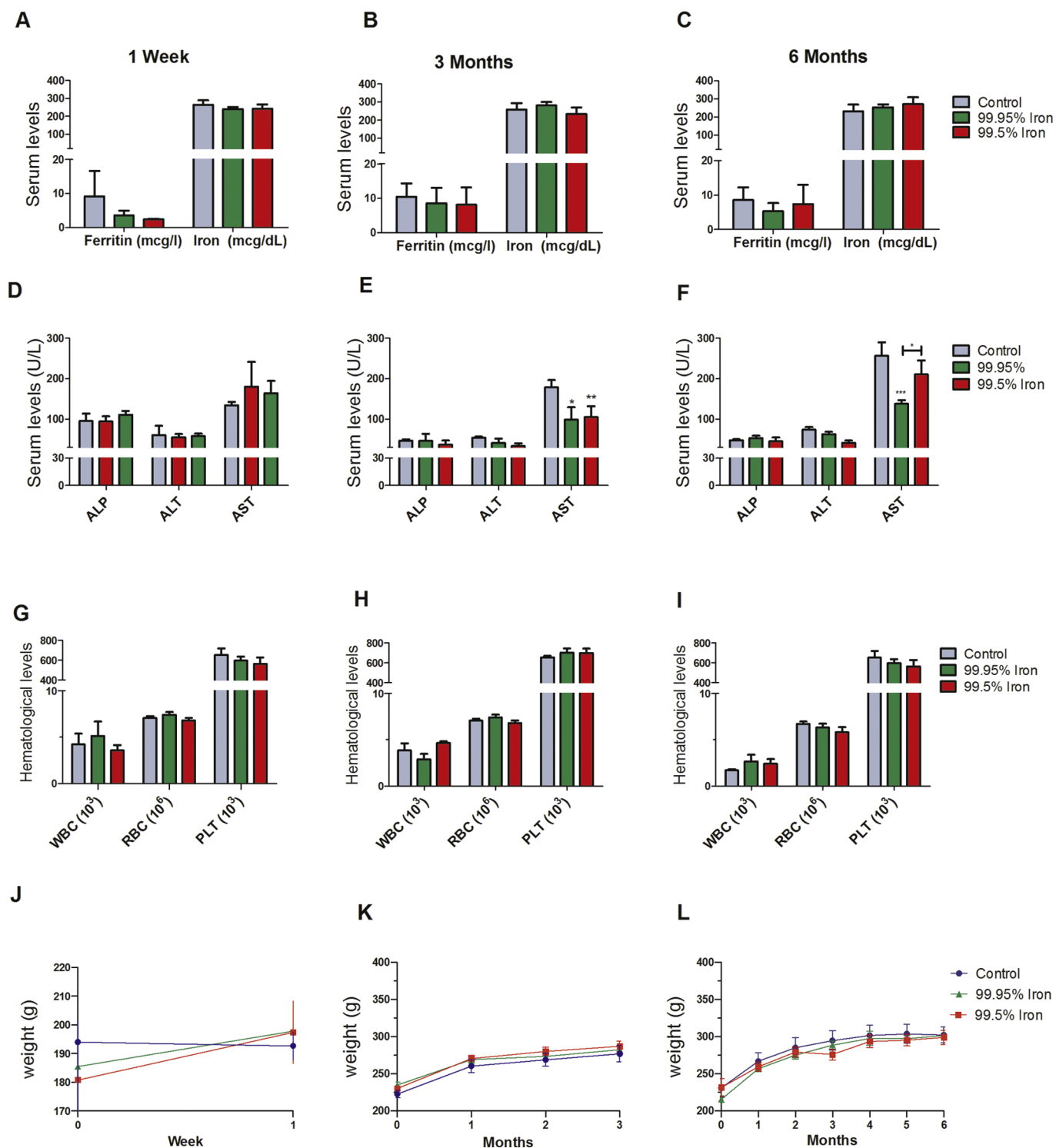
Fig. 8. Serum levels: Ferritin and Iron after 1 week (A), 3 months (B) and 6 months (C). ALP, AST, ALT after 1 week (D), 3 months (E) and 6 months (F). Hematological parameters: Red blood cells (RBC) level (b) Hemoglobin (HGB) level (C) White blood cells (WBC) level after 1 week (G), 3 months (H) and 6 months (I). Body Weight follows after 1 week (J), 3 months (K) and 6 months (L) groups. *represents p < 0.05.

into three categories according to the hemolytic index: hemolytic with a percentage of hemolysis over 5%, slightly hemolytic with a hemolytic index between 5% and 2%, and non-hemolytic with the hemolysis percentage below 2% [37].

The hemolytic index of both irons was lower than 5% indicating their hemocompatibility (Fig. 7). Although, 99.95% iron was less hemolytic than the 99.5% one. The analysis of studies found in the literature showed that pure iron and Fe-based materials caused a

hemolysis percentage ranging from 1.46% to 5.327% [33,34,38,39], corroborating our findings. According to the ASTM standards, 99.95% and 99.5% iron produced by powder metallurgy are potential candidates to be considered for medical applications.

3.5. In vivo biocompatibility

The subcutaneous implantation of 99.5 and 99.95% iron discs into
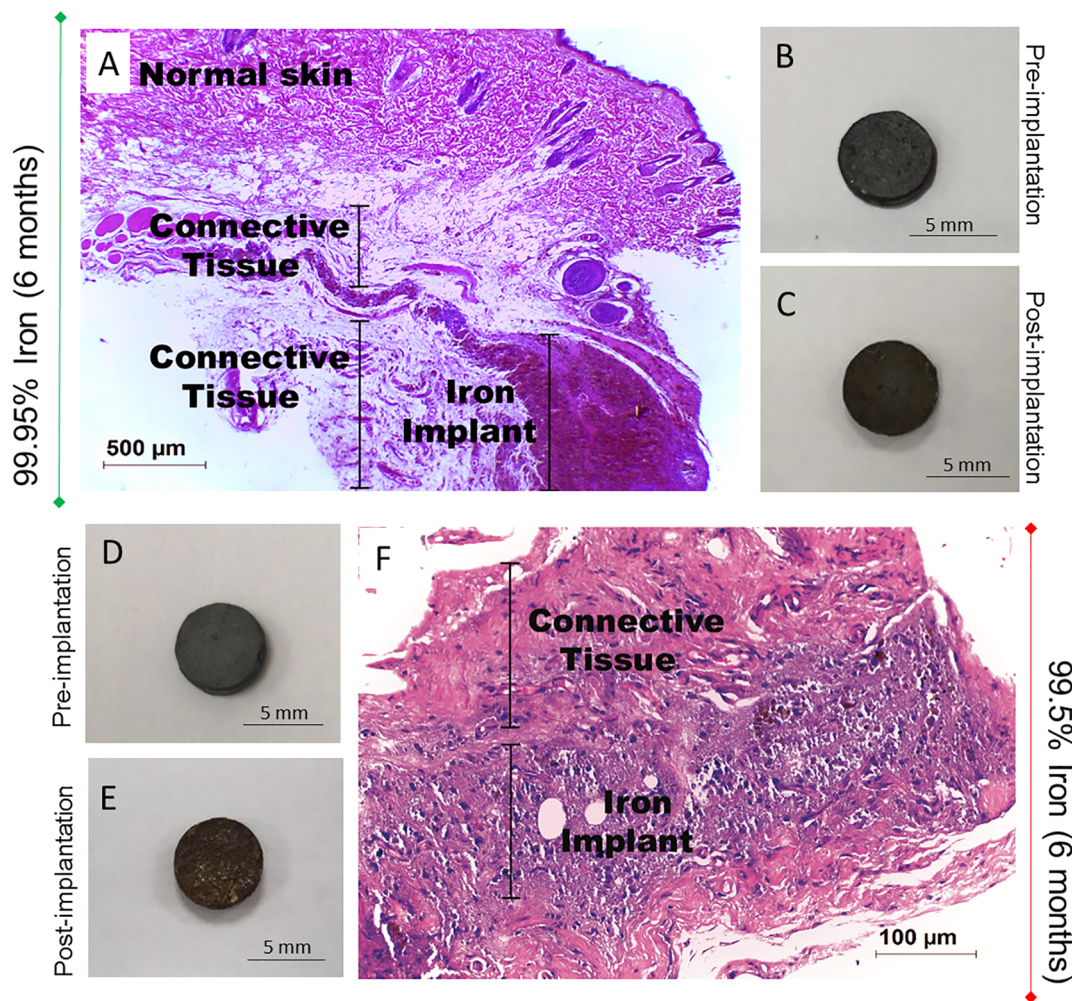
Fig. 9. H&E staining of the subcutaneous tissue around the discs (A, F). 99.95 (B–C) and 99.5% (D–E) iron discs before and after 6 months implantation. The accumulation of iron and the connective tissue that forms in the periphery of the implant were marked in the image.

the dorsal area of rats was performed to evaluate the degradation behavior and biocompatibility under physiological conditions during one week, three and six months.

The ferritin whose major function is to detoxify and store intracellular iron did not show alteration in comparison to control, as well as iron serum levels (Fig. 8A–C) [40]. Serum biochemical and hematological parameters were also analyzed. These analyses revealed similar values for AST, ALT and ALP, when comparing to control and treatments samples (Fig. 8D–F).

RBC, WBC counts and HGB levels in rats implanted with iron discs and controls were similar. This can indicate that the 99.95 and 99.5% iron implants did not cause anemia or general infection (Fig. 8G–I). In addition, all animals with iron implants exhibited normal weight gain, similar to the control group (Fig. 8J–L). Post-implantation assessment including well-being, hair growth and surgical wound healing showed no signs of distress or harmful effects generated by the iron implants.

Histological analysis of the subcutaneous tissue around the iron discs after 6 months are shown in Fig. 9. The implant sites of both irons showed proliferation of fibrous connective tissue, forming a capsule that normally develops around solid, non-corroding or very slow corroding implants [17,41,42]. Subcutaneous tissue and adjacent skin did not present signs of necrosis, but the capsule formed was frequently associated with macrophages with intracytoplasmic granular brownish pigment and occasionally cellular debris and lymphocytes. We neither visualize iron accumulation in the tissues, nor significant changes in the organs (Fig. 10).

Iron stents with 99.8% and 99.5% of purity manufactured by laser cutting processes were implanted, respectively, into the descending aorta of rabbits and minipigs [4,43]. These endovascular stents presented a low thrombogenicity and minimal neointimal hyperplasia. Similarly to our results, in this study, the animals neither showed significant organ accumulation of the degradation products nor systemic and local toxicity. These studies also demonstrated that the degradation rate of iron was low, once large portions of the stents were still intact even after one year of implantation [4,43].

A low degradation rate of iron can prevent fragment embolization in the vase and thus, it is an advantage to use this biomaterial. However, a prolonged degradation time and the difficulty to clear off the degradation products retained in the local tissues are disadvantages of Fe-based metals. The low corrosion can be explained by the formation of an iron oxide passivation layer on the surface that inhibits the chemical attack of the osteogenic body fluid for orthopedic applications and the blood for vascular application [36,44]. To ensure an appropriate degradation rate, it is important to consider the fabrication method and modification of the biomaterial that could accelerate the degradation process, such as surface modification [45], porous ceramic biocomposite [46] and alloying elements [47].

Regarding our study, we also observed a low degradation rate of iron samples implanted in animals, with minimal loss up to six months, without difference between the irons tested (Table 3). In accordance, Drynda and colleagues found that FeMn alloys and pure iron implanted in the subcutaneous tissue of mice did not exhibit significant signs of
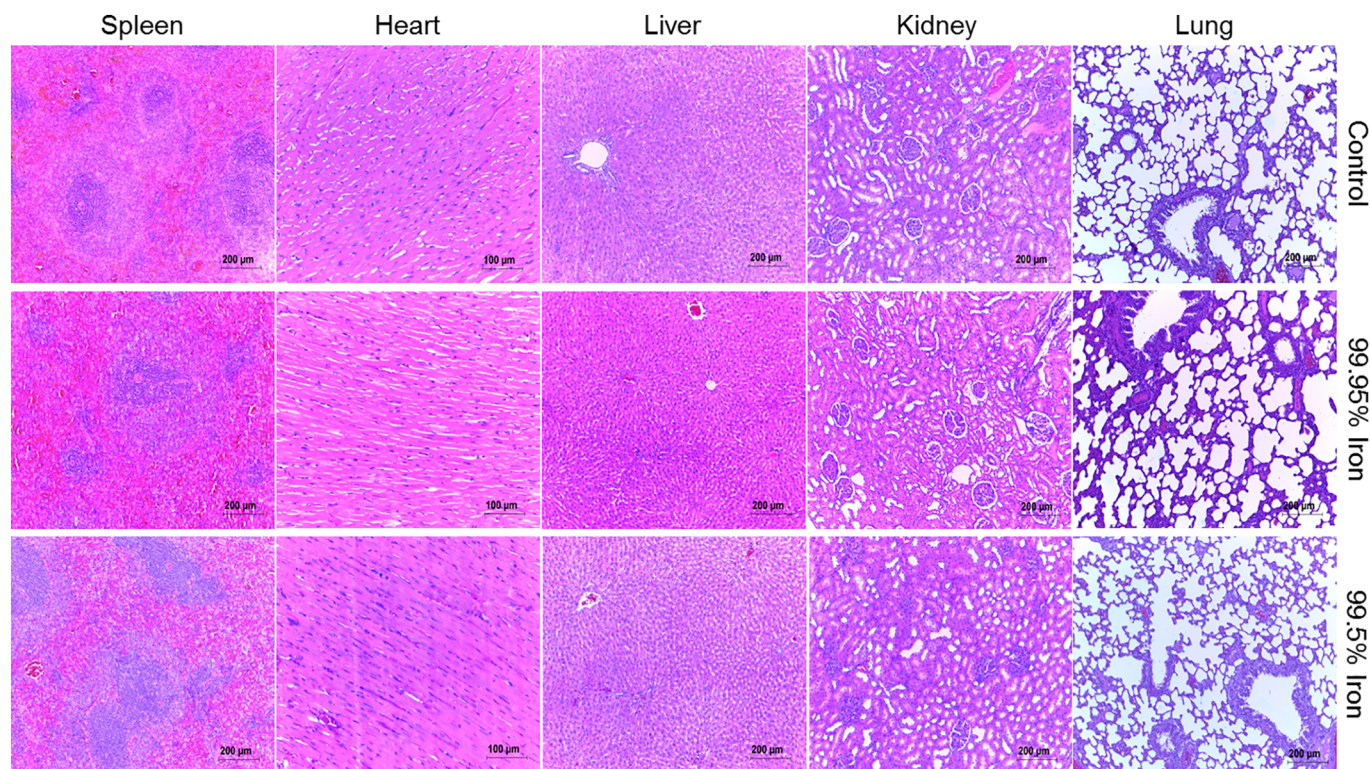
Fig. 10. Histopathology of the major organs after 6 months of iron implantation discs in the subcutaneous tissue. Hematoxylin and eosin staining of tissues harvested from spleen, heart, liver, kidney and lung of the rats. The analysis did not reveal any histological changes between implanted and non-implanted rats.

Table 3
Masses of 99.95 and 99.5% iron discs before and after implantation in the subcutaneous tissue of rats using paired *t*-test.

		99.95% Iron				99.5% Iron		
	N	Average pre implantation (SD)	Average post implantation (SD)	p-Value	N	Average pre implantation (SD)	Average post implantation (SD)	p-Value
6 Months	5	0.455 (0.092)	0.457 (0.093)	0.7077	6	0.371 (0.187)	0.372 (0.189)	0.6432
3 Months	5	0.351 (0.137)	0.351 (0.138)	0.0597	6	0.458 (0.137)	0.458 (0.137)	0.4743
1 Week	6	0.379 (0.073)	0.380 (0.073)	0.0064	6	0.344 (0.106)	0.345 (0.107)	0.0214

Abbreviation: SD = standard deviation.

corrosion after 3, 6, and 9 months [48]. This was expected, once the implants were subcutaneously implanted, avoiding the shear stress. Additionally, other experiments indicated that the degradable rate of pure iron *in vivo* is lower than *in vitro* [32].

A biodegradable metal stent must remain intact in the first 6 months and start its degradation between the 6th and 12th month, which is the interval where the remodeling of the vessel occurs. After this period, the material should progressively increase its degradation [49]. Therefore, the fact that our samples did not show degradation in the first 6 months is a desirable characteristic according to the literature. However, it is important to reinforce a limitation of our study. In our preclinical model, the iron samples were implanted into the subcutaneous of rats, thus avoiding the interaction between the biomaterial and blood vessels. When a stent is expanded in the artery, it is exposed to residual stress, cyclic loading from vessel expansion/contraction, and shear stress by blood flow [50]. These are factors that will influence the degradation rate of the stent.

4. Conclusion

Currently, the manufacturing process of stents involves several steps, such as casting, extrusion and laser cutting of alloys, which lead to an increase in the cost of production. Powder Metallurgy is a relatively recent technique with high precision and productive capacity, in which the loss of raw material used in the manufacturing of the component is minimal or nonexistent [9]. There are few studies in the literature testing pure iron stents and, so far, none testing the powder metallurgy fabrication method [4,43,51,52].

The Food and Drug Administration (FDA) does not approve specific biomaterials for clinical use, as pure iron. The approvals are only issued for clinical use of specific devices [53]. Despite promising, there is no FDA approved iron stent yet. Therefore, results from engineering, *in vitro* and *in vivo* biocompatibility are necessary to prove that this material can be used with safety [54,55]. In this context, our study is important as it showed that the pure iron samples produced by powder metallurgy are biocompatible *in vitro* and *in vivo*. In addition, they have the physical and mechanical properties necessary to encourage the production of medical devices such as stents, which can be tested intravenously in preclinical models, as minipigs that allow to evaluate the degradation rate under shear stress, as well as the other hemodynamic parameters necessary to consider them for clinical trials.

CRediT authorship contribution statement

Thaís Casagrande Paim: Conceptualization, Data curation, Formal analysis, Methodology, Investigation, Visualization, Writing - original draft, Writing - review & editing. **Diego Pacheco Wermuth:** Conceptualization, Data curation, Formal analysis, Methodology, Investigation, Visualization, Writing - original draft, Writing - review & editing. **Isadora Bertaco dos Santos:** Investigation, Validation, Visualization. **Carla Zanatelli:** Conceptualization, Investigation. **Liliana Ivet Sous Naasani:** Conceptualization, Investigation. **Mônica Slaviero:** Investigation, Formal analysis. **David Driemeier:** Formal analysis. **Lirio Schaeffer:** Conceptualization, Funding acquisition, Project administration, Resources, Supervision. **Márcia Rosângela Wink:** Conceptualization, Formal analysis, Methodology, Funding acquisition, Project administration, Resources, Supervision, Writing - original draft, Writing - review & editing.

Declaration of competing interest

The authors declare that they have no known competing financial interests or personal relationships that could have appeared to influence the work reported in this paper.

Acknowledgments

References

[1] N.S. Fagali, C.A. Grillo, S. Puntarulo, M.A. Fernández Lorenzo de Mele, Cytotoxicity of corrosion products of degradable Fe-based stents: relevance of pH and insoluble products, Colloids Surf. B Biointerfaces 128 (2015) 480–488.

[2] A. Purnama, H. Hermawan, J. Couet, D. Mantovani, Assessing the biocompatibility of degradable metallic materials: state-of-the-art and focus on the potential of genetic regulation, Acta Biomater. 6 (2010) 1800–1807.

[3] M. Moravej, D. Mantovani, Biodegradable metals for cardiovascular stent application: interests and new opportunities, Int. J. Mol. Sci. 12 (2011) 4250–4270.

[4] M. Peuster, C. Hesse, T. Schloo, C. Fink, P. Beerbaum, C. von Schnakenburg, Long-term biocompatibility of a corrodible peripheral iron stent in the porcine descending aorta, Biomaterials 27 (2006) 4955–4962.

[5] N. Gonzalo, C. Macaya, Absorbable stent: focus on clinical applications and benefits, Vasc. Health Risk Manag. 8 (2012) 125–132.

[6] H. Hermawan, A. Purnama, D. Dube, J. Couet, D. Mantovani, Fe-Mn alloys for metallic biodegradable stents: degradation and cell viability studies, Acta Biomater. 6 (2010) 1852–1860.

[7] A. Schömig, A. Kastrati, H. Mudra, R. Blasini, H. Schühlen, V. Klauss, G. Richardt, F.J. Neumann, Four-year experience with Palmaz-Schatz stenting in coronary angioplasty complicated by dissection with threatened or present vessel closure, Circulation 90 (1994) 2716–2724.

[8] H. Hermawan, H. Alamdari, D. Mantovani, D. Dubé, Iron–manganese: new class of metallic degradable biomaterials prepared by powder metallurgy, Powder Metall. 51 (2008) 38–45, https://doi.org/10.1179/174329008x284868.

[9] A.C. Tavares, P. Mariot, D.C.L. Luana, L. Schaeffer, Metal injection molding for production of biodegradable implants: an analysis of the potential of pure iron for application in stents, American Journal of Materials Science 9 (2019) 36–43.

[10] J.J. Elsner, A. Kraitzer, O. Grinberg, M. Zilberman, Highly porous drug-eluting structures: from wound dressings to stents and scaffolds for tissue regeneration, Biomatter 2 (2012) 239–270.

[11] H. Hermawan, D. Dubé, D. Mantovani, Degradable metallic biomaterials: design and development of Fe-Mn alloys for stents, J. Biomed. Mater. Res. A 93 (2010) 1–11.

[12] Y. Kohgo, K. Ikuta, T. Ohtake, Y. Torimoto, J. Kato, Body iron metabolism and pathophysiology of iron overload, Int. J. Hematol. 88 (2008) 7–15, https://doi.org/10.1007/s12185-008-0120-5.

[13] E04 Committee, Test Method for Knoop and Vickers Hardness of Materials, ASTM International, West Conshohocken, PA, 2011, https://doi.org/10.1520/E0384-11E01.

[14] E28 Committee, Test Method for Brinell Hardness of Metallic Materials, ASTM International, West Conshohocken, PA, 2015, https://doi.org/10.1520/E0010-15.

[15] E04 Committee, Guide for Preparation of Metallographic Specimens, ASTM International, West Conshohocken, PA, 2011, https://doi.org/10.1520/E0003-11.

[16] E04 Committee, Test Method for Determining Volume Fraction by Systematic Manual Point Count, ASTM International, West Conshohocken, PA, 2019, https://doi.org/10.1520/E0562-19.

[17] C. Rodrigues, L.I.S. Naasani, C. Zanatelli, T.C. Paim, J.G. Azevedo, J.C. de Lima, M. da Cruz Fernandes, S. Buchner, M.R. Wink, Bioglass 45S5: structural characterization of short range order and analysis of biocompatibility with adipose-derived mesenchymal stromal cells in vitro and in vivo, Mater. Sci. Eng. C Mater. Biol. Appl. 103 (2019) 109781.

[18] L.I.S. Naasani, L.I. Sous Naasani, C. Rodrigues, J.G. Azevedo, A.F. Damo Souza, S. Buchner, M.R. Wink, Comparison of human denuded amniotic membrane and porcine small intestine submucosa as scaffolds for limbal mesenchymal stem cells, Stem Cell Rev. Rep. 14 (2018) 744–754, https://doi.org/10.1007/s12015-018-9819-8.

[19] L.R. Beckenkamp, L.E.B. Souza, F.U.F. Melo, C.H. Thomé, D.A.R. Magalhães, P.V.B. Palma, D.T. Covas, Comparative characterization of CD271 and CD271 subpopulations of CD34 human adipose-derived stromal cells, J. Cell. Biochem. 119 (2018) 3873–3884.

[20] A. Schäffler, C. Büchler, Concise review: adipose tissue-derived stromal cells–basic and clinical implications for novel cell-based therapies, Stem Cells 25 (2007) 818–827.

[21] International Organization for Standardization, Biological Evaluation of Medical Devices- Part 12: Sample Preparation and Reference Materials, (2004).

[22] H. Zhu, Cell proliferation assay by flow cytometry (BrdU and PI staining), Bio-protocol 2 (2012), https://doi.org/10.21769/BioProtoc.198.

[23] V. Vichai, K. Kirtikara, Sulforhodamine B colorimetric assay for cytotoxicity screening, Nat. Protoc. 1 (2006) 1112–1116.

[24] L. Mota Ferreira, M. Gehrcke, V. Ferrari Cervi, P. Eliete Rodrigues Bitencourt, E. Ferreira da Silveira, J. Hofstatter Azambuja, A. Prates Ramos, K. Nascimento, M. Beatriz Moretto, E. Braganhol, M. Rorato Sagrillo, L. Cruz, Pomegranate seed oil nanoemulsions with selective antiglioma activity: optimization and evaluation of cytotoxicity, genotoxicity and oxidative effects on mononuclear cells, Pharm. Biol. 54 (2016) 2968–2977.

[25] E. Zhang, H. Chen, F. Shen, Biocorrosion properties and blood and cell compatibility of pure iron as a biodegradable biomaterial, J. Mater. Sci. Mater. Med. 21 (2010) 2151–2163.

[26] R.M. German, Powder Metallurgy Science, Metal Powder Industry, (1994).

[27] N. Baltzer, T. Copponnex, Properties and processing of precious metal alloys for biomedical applications, Precious Metals for Biomedical Applications, 2014, pp. 3–36, , https://doi.org/10.1533/9780857099051.1.3.

[28] S. Wang, X. Zhang, J. Li, C. Liu, S. Guan, Investigation of Mg-Zn-Y-Nd alloy for potential application of biodegradable esophageal stent material, Bioact. Mater. 5 (2020) 1–8.

[29] X.N. Gu, W.R. Zhou, Y.F. Zheng, Y. Cheng, S.C. Wei, S.P. Zhong, T.F. Xi, L.J. Chen, Corrosion fatigue behaviors of two biomedical Mg alloys – AZ91D and WE43 – in simulated body fluid, Acta Biomater. 6 (2010) 4605–4613, https://doi.org/10.1016/j.actbio.2010.07.026.

[30] M. Dominici, K. Le Blanc, I. Mueller, I. Slaper-Cortenbach, F. Marini, D. Krause, R. Deans, A. Keating, D. Prockop, E. Horwitz, Minimal criteria for defining multi-potent mesenchymal stromal cells. The International Society for Cellular Therapy position statement, Cytotherapy 8 (2006) 315–317.

[31] N.M. Daud, N.B. Sing, A.H. Yusop, F.A.A. Majid, H. Hermawan, Degradation and in vitro cell–material interaction studies on hydroxyapatite-coated biodegradable porous iron for hard tissue scaffolds, Journal of Orthopaedic Translation 2 (2014) 177–184, https://doi.org/10.1016/j.jot.2014.07.001.

[32] S. Zhu, N. Huang, L. Xu, Y. Zhang, H. Liu, H. Sun, Y. Leng, Biocompatibility of pure iron: in vitro assessment of degradation kinetics and cytotoxicity on endothelial cells, Mater. Sci. Eng. C 29 (2009) 1589–1592, https://doi.org/10.1016/j.msec.2008.12.019.

[33] J. Cheng, T. Huang, Y.F. Zheng, Microstructure, mechanical property, biodegradation behavior, and biocompatibility of biodegradable Fe-Fe2O3 composites, J. Biomed. Mater. Res. A 102 (2014) 2277–2287.

[34] B. Liu, Y.F. Zheng, Effects of alloying elements (Mn, Co, Al, W, Sn, B, C and S) on biodegradability and in vitro biocompatibility of pure iron, Acta Biomater. 7 (2011)

1407–1420, https://doi.org/10.1016/j.actbio.2010.11.001.

[35] S. Bagherifard, M.F. Molla, D. Kajanek, R. Donnini, B. Hadzima, M. Guagliano, Accelerated biodegradation and improved mechanical performance of pure iron through surface grain refinement, Acta Biomater. 98 (2019) 88–102.

[36] A.H.M. Yusop, N.M. Daud, H. Nur, M.R.A. Kadir, H. Hermawan, Controlling the degradation kinetics of porous iron by poly(lactic-co-glycolic acid) infiltration for use as temporary medical implants, Sci. Rep. 5 (2015) 11194.

[37] ASTM International, Standard Practice for Assessment of Hemolytic Properties of Materials, West Conshohocken, PA, (2008), https://doi.org/10.1520/f0756-08.

[38] A. Oriňák, R. Oriňáková, Z.O. Králová, A.M. Turoňová, M. Kupková, M. Hrubovčáková, J. Radoňák, R. Džunda, Sintered metallic foams for biodegradable bone replacement materials, J. Porous. Mater. 21 (2014) 131–140, https://doi.org/10.1007/s10934-013-9757-4.

[39] H. Chen, E. Zhang, K. Yang, Microstructure, corrosion properties and bio-compatibility of calcium zinc phosphate coating on pure iron for biomedical application, Mater. Sci. Eng. C Mater. Biol. Appl. 34 (2014) 201–206.

[40] K. Watanabe, Y. Yamashita, H. Ohgawara, M. Sekiguchi, N. Satake, K. Orino, S. Yamamoto, Iron content of rat serum ferritin, J. Vet. Med. Sci. 63 (2001) 587–589, https://doi.org/10.1292/jvms.63.587.

[41] E. Willbold, K. Kalla, I. Bartsch, K. Bobe, M. Brauneis, S. Remennik, D. Shechtman, J. Nellesen, W. Tillmann, C. Vogt, F. Witte, Biocompatibility of rapidly solidified magnesium alloy RS66 as a temporary biodegradable metal, Acta Biomater. 9 (2013) 8509–8517.

[42] A. Drynda, J. Seibt, T. Hassel, F.W. Bach, M. Peuster, Biocompatibility of fluoride-coated magnesium-calcium alloys with optimized degradation kinetics in a subcutaneous mouse model, J. Biomed. Mater. Res. A 101A (2013) 33–43, https://doi.org/10.1002/jbm.a.34300.

[43] M. Peuster, P. Wohlsein, M. Brügmann, M. Ehlerding, K. Seidler, C. Fink, H. Brauer, A. Fischer, G. Hausdorf, A novel approach to temporary stenting: degradable cardiovascular stents produced from corrodible metal-results 6-18 months after implantation into New Zealand white rabbits, Heart 86 (2001) 563–569.

[44] D. Zhu, I. Cockerill, Y. Su, Z. Zhang, J. Fu, K.-W. Lee, J. Ma, C. Okpokwasili, L. Tang, Y. Zheng, Y.-X. Qin, Y. Wang, Mechanical strength, biodegradation, and in vitro and

in vivo biocompatibility of Zn biomaterials, ACS Appl. Mater. Interfaces 11 (2019) 6809–6819.

[45] Y. Qi, X. Li, Y. He, D. Zhang, J. Ding, Mechanism of acceleration of Iron corrosion by a polylactide coating, ACS Appl. Mater. Interfaces 11 (2019) 202–218.

[46] M. Heiden, E. Nauman, L. Stanciu, Bioresorbable Fe-Mn and Fe-Mn-HA materials for orthopedic implantation: enhancing degradation through porosity control, Adv. Healthc. Mater. 6 (2017), https://doi.org/10.1002/adhm.201700120.

[47] M. Schinhammer, A.C. Hänzi, J.F. Löffler, P.J. Uggowitzer, Design strategy for biodegradable Fe-based alloys for medical applications, Acta Biomater. 6 (2010) 1705–1713.

[48] A. Drynda, T. Hassel, F.W. Bach, M. Peuster, In vitro and in vivo corrosion properties of new iron-manganese alloys designed for cardiovascular applications, J Biomed Mater Res B Appl Biomater 103 (2015) 649–660.

[49] H. Hermawan, D. Dubé, D. Mantovani, Degradable metallic biomaterials for cardiovascular applications, Metals for Biomedical Devices (2010) 379–404, https://doi.org/10.1533/9781845699246.4.379.

[50] Y. Koo, T. Tiasha, V.N. Shanov, Y. Yun, Expandable mg-based helical stent assessment using static, dynamic, and porcine ex vivo models, Sci. Rep. 7 (2017) 1173.

[51] R. Waksman, R. Pakala, R. Baffour, R. Seabron, D. Hellinga, F.O. Tio, Short-term effects of biocorrodible iron stents in porcine coronary arteries, J. Interv. Cardiol. 21 (2008) 15–20.

[52] H. Hermawan, D. Dubé, D. Mantovani, Developments in metallic biodegradable stents, Acta Biomater. 6 (2010) 1693–1697.

[53] A.S. Hoffman, The History and Evolution of Biomaterials and Medical Devices, Slabo. (n.d.). http://slabo.org.br/the-history-and-evolution-of-biomaterials-and-medical-devices/ (accessed April 21, 2020).

[54] Center for Devices, Radiological Health, Metals Used in Medical Devices, U.S. Food and Drug Administration, 2020, https://www.fda.gov/medical-devices/products-and-medical-procedures/metals-used-medical-devices , Accessed date: 17 April 2020.

[55] Q. Chen, G.A. Thouas, Metallic implant biomaterials, Materials Science and Engineering: R: Reports 87 (2015) 1–57, https://doi.org/10.1016/j.mser.2014.10.001.